Inorganic Chemistry
Article
pubs.acs.org/IC

Synthesis and Selective CO_2 Capture Properties of a Series of Hexatopic Linker-Based Metal–Organic Frameworks

Phuong T. K. Nguyen,[†,§] Huong T. D. Nguyen,[†,‡,§] Hung Q. Pham,[†,‡] Jaheon Kim,[#] Kyle E. Cordova,*[,†,⊥] and Hiroyasu Furukawa*[,⊥,∥]

[†]Center for Molecular NanoArchitecture and [‡]Faculty of Chemistry, University of Science, Vietnam National University—Ho Chi Minh City (VNU—HCM), Ho Chi Minh City 721337, Vietnam

[#]Department of Chemistry, Soongsil University, 369 Sangdo-Ro, Dongjak-Gu, Seoul 156-743, Republic of Korea

[⊥]Department of Chemistry and Materials Sciences Division, Lawrence Berkeley National Laboratory, and Center for Global Science at Berkeley, University of California—Berkeley, Berkeley, California 94720, United States

[∥]King Fahd University of Petroleum and Minerals, Dhahran 34464, Saudi Arabia

Supporting Information

ABSTRACT: Four crystalline, porous metal–organic frameworks (MOFs), based on a new hexatopic linker, 1′,2′,3′,4′,5′,6′-hexakis(4-carboxyphenyl)-benzene (H_6CPB), were synthesized and fully characterized. Interestingly, two members of this series exhibited new topologies, namely, **htp** and **hhp**, which were previously unseen in MOF chemistry. Gas adsorption measurements revealed that all members exhibited high CO_2 selectivity over N_2 and CH_4. Accordingly, breakthrough measurements were performed on a representative example, in which the effective separation of CO_2 from binary mixtures containing either N_2 or CH_4 was demonstrated without any loss in performance over three consecutive cycles.

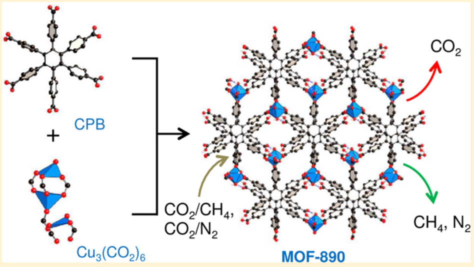

INTRODUCTION

Metal–organic frameworks (MOFs) are constructed via strong bonds between metal-containing clusters and organic linkers, both of which are termed secondary building units (SBUs).[1] Through the use of reticular chemistry, it is well understood that MOFs can be designed based on geometrically influenced choices of inorganic and organic building units.[1,2] The resulting crystalline structures have attracted much promise in a wide range of applications, including gas storage and separations, heterogeneous catalysis, conductivity, and water storage.[3−6]

One particular direction that has received attention in MOF synthesis is the use of multicarboxylate organic linkers, which has afforded new MOF materials with unique structural features and interesting intrinsic properties.[7,8] Specifically, when multicarboxylate linkers are employed, the metrics of the pore size and shape as well as the pore surface have been shown to be modifiable to optimize for gas storage and separation applications. The first example of using a multicarboxylate linker in MOF synthesis was MODF-1 (where MODF-1 = metal–organic dendrimer framework-1), in which a dendritic hexacarboxylate (hexatopic) linker was used to construct a permanently porous structure with **NiAs** topology.[9] The reporting of UTSA-62a also demonstrated the use of a dendritic hexatopic linker, leading to a highly porous framework with low interactions with CO_2.[10] These favorable properties afforded UTSA-62a as an effective adsorbent for H_2 purification purposes.[10] NU-110E, constructed from an elongated hexatopic linker, demonstrated the highest Brunauer–Emmett–Teller (BET) surface area (7140 m^2 g^{-1}) for any known porous material.[11] Hexatopic linkers were also utilized in the synthesis of the ultrahighly porous PCN-69 (also known as NOTT-119), as well as NOTT-112, NU-100, and NU-111.[12] The synthesis of an isoreticular (having the same topology) series of MOFs from a different dendritic hexatopic linker, termed JUC-100, JUC-103, and JUC-106, was shown to combine high porosity with suitable pore sizes for light hydrocarbon separation.[13] Similarly, a series of isoreticular MOFs (PCN-61, -66, -68, and -610) was produced from novel hexatopic linkers, affording structures with high porosity and high gas adsorption properties.[14] It is noted that a limited number of MOF architectures built from octatopic and dodecatopic linkers have also been reported.[15,16]

To further explore the construction of MOFs based on multicarboxylate linkers, we describe the synthesis of a new hexatopic linker, 1′,2′,3′,4′,5′,6′-hexakis(4-carboxyphenyl)-benzene (H_6CPB; Scheme 1).[17] It is worth noting that the H_6CPB linker was designed to be highly symmetrical, in which the local C_2 axes of the aryl faces form 60° angles with respect to one another. With this new linker in hand, we further report the synthesis and characterization of a series of four new MOFs, including $[Ni_2(CPB)]\cdot 4.1H_2O$, $[Mg_2(H_2CPB)(DEF)_{0.5}(EtOH)_{0.5}]\cdot 3H_2O$, $[Cu_3(CPB)(DMF)_{0.5}]\cdot 6H_2O$, and $[Cu_3(CPB)(DEF)_{0.4}]\cdot 3.8H_2O$ (termed MOF-888, -889, -890,

Received: August 18, 2015
Published: October 7, 2015

ACS Publications © 2015 American Chemical Society

DOI: 10.1021/acs.inorgchem.5b01900
Inorg. Chem. 2015, 54, 10065−10072

Scheme 1. Hexatopic Linker CPB Used in This Work

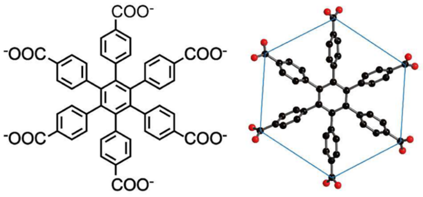

and -891, respectively, where DEF = *N*,*N*-diethylformamide, EtOH = ethanol, and DMF = *N*,*N*-dimethylformamide), and describe their gas adsorption properties. Within this series, the structural frameworks were shown to vary from two-dimensional (2D) layers (MOF-888) to three-dimensional (3D) architectures (MOF-889 to -891). Finally, we demonstrate that MOF-890 is an effective adsorbent for the dynamic separation of CO_2 from binary mixtures containing N_2 or CH_4.

■ EXPERIMENTAL SECTION

Materials and General Procedures. Full synthetic and characterization details can be found in the Supporting Information (SI), sections S1 and S2. Copper(II) nitrate trihydrate, nickel(II) acetate tetrahydrate, magnesium nitrate hexahydrate, anhydrous DMF, and DEF were obtained from Sigma-Aldrich. Anhydrous dichloromethane (DCM), methanol (MeOH), and EtOH were purchased from Acros Organics. Deionized water was obtained from a Barnstead Easypure II (17.8 MΩ·cm resistivity). All chemicals, unless otherwise specified, were used without further purification.

Elemental microanalyses (EA) were performed in the Microanalytical Laboratory of the College of Chemistry at University of California—Berkeley, using a PerkinElmer 2400 series II CHNS elemental analyzer. Fourier transform infrared (FT-IR) spectra were measured using KBr pellets on a Bruker Vertex 70 system, and the output signals are described as follows: vs, very strong; s, strong; m, medium; sh, shoulder; w, weak; vw, very weak; br, broad. Thermal gravimetric analysis (TGA) was performed on a TA Q500 thermal analysis system with the sample held in a platinum pan in a continuous airflow. Low-pressure N_2, CO_2, and CH_4 adsorption isotherms were recorded on a Micromeritics 3Flex. A liquid-N_2 bath was used for measurements at 77 K, and a water circulator was used for measurements at 273, 283, and 298 K. For all sorption measurements, He was used to estimate the dead space. Breakthrough measurements were performed using a L&C Science and Technology PSA-300-LC analyzer. The bed column dimensions were l × i.d. = 14 cm × 0.635 cm. The gaseous effluent from the sample bed was monitored for CO_2, CH_4, N_2, H_2O, and O_2 by a ThermoStar GSD320 mass spectrometer. Ultrahigh-purity-grade N_2, CH_4, and He gases (99.999% purity) as well as high-purity-grade CO_2 (99.995%) were used throughout the experiments.

Synthesis of the Hexatopic Linker 1′,2′,3′,4′,5′,6′-Hexakis(4-carboxyphenyl)benzene (H_6CPB). H_6CPB was synthesized via a one-pot Sonogashira coupling reaction, followed by a Co-catalyzed cyclotrimerization, and subsequent hydrolysis to produce the resulting H_6CPB linker (Scheme 1).[17] Full synthetic details are described in the SI, section S2.

X-ray Diffraction Analysis. Single-crystal X-ray diffraction (SCXRD) analysis was performed on a Bruker D8 Venture diffractometer using monochromatic fine-focus Cu Kα radiation (λ = 1.54178 Å). The measurements were operated at 50 kV and 1.0 mA using a Photon 100 CMOS detector at 100 K for MOF-888, -890, and -891 and at 298 K for MOF-889. The data were collected with ϕ and ω scans using a narrow-frame algorithm. The frames were integrated using the Bruker *SAINT* software package. The reflection data were corrected for absorption by using Bruker *SADABS*, solved with the Bruker *SHELXTL* software package using direct methods and refined by full-matrix least-squares techniques against F^2 with the *SHELXL* program package. To improve the refinement, the *SQUEEZE* routine within the *PLATON* software package was used to treat the unidentified occluded solvent molecules. Full SCXRD analysis details can be found in the SI, section S3. Powder X-ray diffraction (PXRD) patterns were recorded using a Bruker D8 Advance diffractometer with Ni-filtered Cu Kα radiation (λ = 1.54178 Å). The system was also outfitted with an antiscattering shield that prevents incident diffuse radiation from hitting the detector. Samples were placed on zero background sample holders by dropping powders and then leveling the sample with a spatula. The 2θ range was 3−50° with a scan speed of 1 s step^{-1} and a step size of 0.02°.

Synthesis of MOF-888, $[Ni_2(CPB)]\cdot 4.1H_2O$. A 0.05 M stock solution of nickel(II) acetate tetrahydrate in DMF (0.375 mL) was added to a 2 mL Pyrex tube (o.d. × i.d. = 6.5 mm × 5.5 mm), which was preloaded with H_6CPB (15 mg, 0.019 mmol). This was followed by the addition of 1.125 mL of deionized water. The tube was then quickly sealed, sonicated for 5 min, and heated at 150 °C for 48 h to produce yellow rectangular-shaped crystals. The crystals were then thoroughly washed with DMF (4 × 5 mL) per day for a total of 3 days. To yield guest-free material, DMF-washed MOF-888 was subsequently immersed in DCM (4 × 5 mL) per day over a period of 4 days. The solvent-exchanged sample was activated under vacuum at ambient temperature for 24 h, followed by heating at 240 °C under vacuum for an additional 24 h. EA. Calcd for $Ni_2C_{48}H_{32.20}O_{16.10}$ ($[Ni_2(CPB)]\cdot 4.1H_2O$): C, 58.59; H, 3.30. Found: C, 58.55; H, 3.63. FT-IR (KBr, 3500−400 cm^{-1}): 3430 (br), 3066 (w), 2802 (vw), 2361 (vw), 1699 (w), 1609 (m), 1584 (m), 1524 (m), 1427 (s), 1411 (s), 1309 (vw), 1277 (br), 1180 (w), 1150 (vw), 1101 (br), 1018 (w), 866 (s), 758 (s).

Synthesis of MOF-889, $[Mg_2(H_2CPB)(DEF)_{0.5}(EtOH)_{0.5}]\cdot 3H_2O$. A 0.5 M stock solution of magnesium nitrate hexahydrate in deionized water (0.12 mL) was added to an 8 mL vial, which was preloaded with H_6CPB (8 mg, 0.01 mmol). This was followed by the addition of DEF (0.40 mL), EtOH (1.50 mL), and deionized water (0.24 mL) to the vial. The reaction mixture was quickly sonicated and heated at 120 °C for 24 h, yielding colorless, block-shaped crystals. The crystals were then thoroughly washed with DMF (4 × 8 mL) per day for 4 days total. To yield guest-free material, DMF-washed MOF-889 was subsequently immersed in DCM (4 × 8 mL) per day for 4 days total. The solvent-exchanged sample was activated under vacuum at ambient temperature for 24 h, followed by heating at 180 °C under vacuum for an additional 24 h. EA. Calcd for $Mg_2C_{50.5}H_{37.50}O_{15.50}N_{0.5}$ ($[Mg_2(H_2CPB)(DEF)_{0.5}(EtOH)_{0.5}]\cdot 3H_2O$): C, 63.70; H, 3.99; N, 0.74. Found: C, 63.61; H, 3.60; N, 0.48. FT-IR (KBr, 3500−400 cm^{-1}): 3417 (br), 2975 (vw), 2513 (vw), 1696 (m), 1609 (s), 1541 (m), 1405 (s), 1311 (vw), 1277 (br), 1177 (w), 1149 (vw), 1103 (br), 1018 (w), 866 (w), 744 (s).

Synthesis of MOF-890, $[Cu_3(CPB)(DMF)_{0.5}]\cdot 6H_2O$. A 0.165 M stock solution of copper nitrate trihydrate in DMF (0.5 mL) was added to an 8 mL vial, which was preloaded with H_6CPB (20 mg, 0.025 mmol). This was followed by the addition of deionized water (4 mL) to the mixture, which was subsequently heated at 100 °C for 18 h to yield blue, block-shaped crystals. The crystals were then thoroughly washed with DMF (3 × 10 mL) per day for 3 days total. To yield guest-free material, DMF-washed MOF-890 was immersed in MeOH (3 × 10 mL) per day for a total of 4 days. The solvent-exchanged sample was activated under vacuum at ambient temperature for 24 h, followed by heating at 180 °C under vacuum for an additional 24 h. EA. Calcd for $Cu_3C_{48}H_{33.40}O_{16.70}$ ($[Cu_3(CPB)(DMF)_{0.5}]\cdot 6H_2O$): C, 52.71; H, 3.53; N, 0.62. Found: C, 52.10; H, 2.71; N, 0.63. FT-IR (KBr, 3500−400 cm^{-1}): 3429 (br), 1608 (s), 1540 (m), 1404 (br), 1277 (vw), 1180 (w), 1017 (m), 860 (m), 752 (m).

Synthesis of MOF-891, $[Cu_3(CPB)(DEF)_{0.4}]\cdot 3.8H_2O$. A 0.02 M stock solution of copper nitrate trihydrate in DEF (0.5 mL) was added to a 8 mL vial, which was preloaded with H_6CPB (20 mg, 0.025 mmol). This was followed by the addition of deionized water (3 mL) to the mixture, which was then heated at 85 °C for 16 h to yield blue, block-shaped crystals. The crystals were then thoroughly washed with DMF (3 × 10 mL) per day for 3 days total. To yield guest-free material, DMF-washed MOF-891 was immersed in MeOH (3 × 10 mL) per day over a total of 4 days. The solvent-exchanged sample was

Table 1. Crystal Structure Data and Refinement for MOF-888, MOF-889, MOF-890, and MOF-891

	MOF-888	MOF-889	MOF-890	MOF-891
empirical formula	$C_{48}H_{24}O_{12}Ni_2$	$C_{59}H_{55}NO_{16}Mg_2$	$C_{57}H_{47}N_3O_{16}Cu_3$	$C_{63}H_{61}N_3O_{17}Cu_3$
fw (g mol^{-1})	910.09	1082.66	1220.59	1322.76
cryst syst	monoclinic	monoclinic	orthorhombic	triclinic
space group	$C2/c$	$P2_1/n$	$P2_12_12_1$	$P\bar{1}$
a (Å)	16.2264(3)	11.8582(6)	11.540(3)	12.6325(4)
b (Å)	29.4379(6)	28.0640(12)	16.778(6)	17.4726(6)
c (Å)	12.4371(3)	16.7331(8)	28.468(3)	27.9667(9)
α (deg)	90	90	90	91.275(2)
β (deg)	29.4379(6)	96.876(2)	90	92.433(2)
γ (deg)	90	90	90	106.100(2)
V (Å^3)	4980.83(19)	5528.5(5)	5512(3)	5921.7(3)
Z	4	4	4	4
ρ_{calcd} (g cm^{-3})	1.214	1.301	1.471	1.484
μ(Cu Kα) (mm^{-1})	1.405	0.984	1.956	1.878
R_{int}	0.0855	0.0404	0.0910	0.0727
R_1[a]	0.0550	0.0977	0.1289	0.1072
wR_2[b]	0.1363	0.2409	0.3090	0.2100

[a] $R_1 = \sum||F_o| - |F_c||/\sum|F_o|$. [b] $wR_2 = [\sum w(F_o^2 - F_c^2)^2/w(F_o)^2]^{1/2}$ for 3397 reflections satisfying $I > 2\sigma(I)$ (MOF-888), for 2590 reflections satisfying $I > 2\sigma(I)$ (MOF-889), for 2194 reflections satisfying $I > 2\sigma(I)$ (MOF-890), and for 3397 reflections satisfying $I > 2\sigma(I)$ (MOF-891).

activated under vacuum at ambient temperature for 24 h, followed by heating at 180 °C under vacuum for an additional 24 h. EA. Calcd for $Cu_3C_{63}H_{61}O_{17}N_3$ ($[Cu_3(CPB)(DEF)_{0.4}]\cdot 3.8H_2O$): C, 54.98; H, 3.32; N, 0.51. Found: C, 54.67; H, 2.97; N, <0.2. FT-IR (KBr, 3500−400 cm^{-1}): 3433 (br), 2921 (vw), 1609 (m), 1542 (w), 1405 (br), 1179 (vw), 1153 (vw), 1104 (w), 1017 (w), 865 (m), 792 (m).

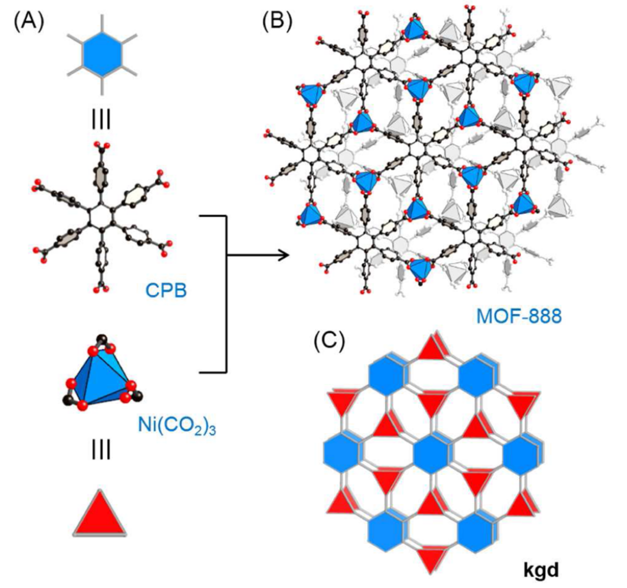

Figure 1. Crystal structure of MOF-888. (A) Linking of hexagonal CPB and triangular $Ni(CO_2)_3$ SBUs resulting in (B) MOF-888. (C) Structure of MOF-888 adopting the **kgd** topology. Color code: Ni, blue polyhedra; C, black, O, red. All H atoms are omitted for clarity.

■ RESULTS AND DISCUSSION

1. Crystal Structures of MOF-888−MOF-891. All bonds in the single-crystal structures of MOF-888−MOF-891 were rigorously elucidated using bond-valence theory before the topological type was determined.[18] Special attention was paid to hydrogen and metal−O bonds because these played a significant role in determining the underlying net of the resulting MOF frameworks. The *TOPOS4.0* package was employed to simplify the structures and to identify the respective underlying net. Details are described in the SI, section S4.[19]

MOF-888. SCXRD analysis revealed that MOF-888 crystallizes in the monoclinic $C2/c$ space group with a = 16.226 Å, b = 29.438 Å, and c = 12.437 Å (Table 1). The framework of MOF-888 is composed of single-metal Ni units with three points of extension resulting from bidentate-coordinated carboxylate functionalities of the CPB linkers (Figure 1A). The overall extended structure can be described as 2D layers that adopt the **kgd** topology as a result of linking triangular (Ni units) and hexagonal (CPB linkers) SBUs together (Figure 1B,C). Interestingly, charge-balance analysis on the Ni SBUs indicates that the oxidation state of Ni must be 3+, which is rather uncommon but not unprecedented (SI, section S4).[20] It is noted that a carboxylate functionality in the CPB linker can potentially exist in protonated form to afford the Ni atoms with the more common oxidation state of 2+. However, the fact that all six Ni−O bond lengths are virtually equal excludes such a possibility.

MOF-889. MOF-889 crystallizes in the monoclinic $P2_1/n$ space group with a = 11.858 Å, b = 28.064 Å, and c = 16.733 Å (Table 1). A combination of SCXRD and charge-balance analyses indicates that only four of the six carboxylic acid moieties of the CPB linker are fully deprotonated. Of these four carboxylates, three form bridging coordinate covalent bonds with two Mg atoms. The fourth carboxylate binds in a monodentate fashion and participates in hydrogen bonding (center-to-center oxygen distance in the range of 2.617−2.847 Å) with the remaining two carboxylic acid functionalities of the CPB linker and two EtOH ligands. Taken together, this produces hydrogen-bonded discrete $Mg_2(CO_2)_4(CO_2H)_2$-$(EtOH)_2$ clusters that arrange in infinite $[Mg_2(CO_2)_4(CO_2H)_2$-$(EtOH)_2]_\infty$ rod-shaped SBUs (Figure 2A). It is noted that one DEF ligand is also present to complete the coordination sphere, but does not play a role in the formation of the rod-shaped SBUs. Topological analysis reveals that the 3D MOF-889 framework adopts the **yav** topology because of the linking of infinite binodal rod-shaped SBUs with hexagonal CPB linker SBUs (Figure 2B,C and SI, section S4).

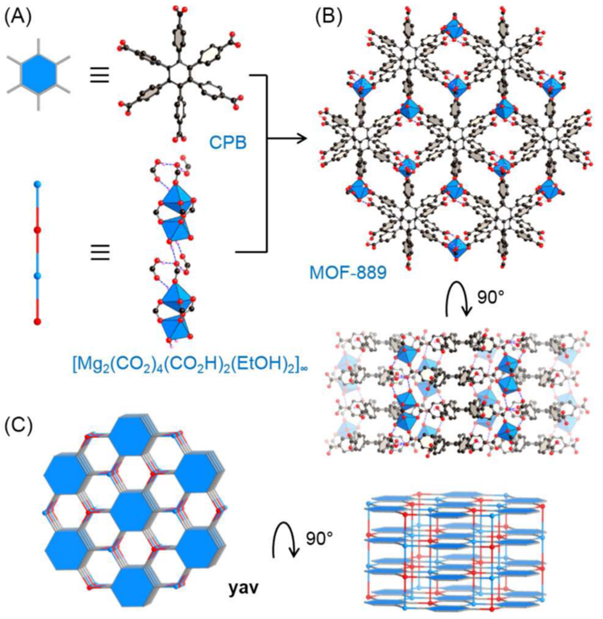

Figure 2. Crystal structure of MOF-889. (A) Linking of hexagonal CPB and infinite $[Mg_2(CO_2)_4(CO_2H)_2(EtOH)_2]_\infty$ (red and blue binodal rods) SBUs resulting in (B) MOF-889. (C) Structure of MOF-889 adopting the **yav** topology. Color code: Mg, blue polyhedra; C, black, O, red. All H atoms, except for those participating in hydrogen bonding, are omitted for clarity.

MOF-890. SCXRD analysis revealed that MOF-890 crystallizes in the orthorhombic $P2_12_12_1$ space group with a = 11.540 Å, b = 16.778 Å, and c = 28.468 Å (Table 1). In this structure, all carboxylate groups of the CPB linker are fully deprotonated to yield discrete $Cu_3(CO_2)_6$ SBUs (Figure 3A). Three carboxylate functionalities coordinate in a bridging fashion to two Cu atoms, and one carboxylate functionality bridges these two Cu atoms to the third Cu atom, which has the final two carboxylate atoms coordinated in a monodentate fashion. DMF and water molecules complete the coordination spheres of the Cu atoms. Considering that the CPB linkers are the points of extension, the $Cu_3(CO_2)_6$ SBUs can be viewed as trigonal prisms (Figure 3A). Accordingly, the resulting 3D framework adopts a new (6,6)-connected **htp** topology. MOF-890 is the first framework with a topology composed of both hexagonal and trigonal-prismatic SBUs (SI, section S4).

MOF-891. SCXRD analysis revealed that MOF-891 crystallizes in the triclinic $P\bar{1}$ space group with unit cell parameters a = 12.633 Å, b = 17.473 Å, and c = 27.967 Å (Table 1). In MOF-891, there exist two types of Cu_3 SBUs, one discrete and one that can be described as an infinite rod (Figure 4A). The discrete Cu_3 cluster, $Cu_3(CO_2)_6(H_2O)_2$, is formed through hydrogen bonding of two smaller charged clusters, notably, $[Cu_2(CO_2)_3(H_2O)]^+$ and $[Cu(CO_2)_3(H_2O)]^-$ (Figure 4A). Topological analysis reveals that these discrete clusters have six points of extension and can be viewed as trigonal prisms. In a similar fashion, the infinite Cu_3 rods, $[Cu_3(CO_2)_6(H_2O)_2]_\infty$, are also formed via hydrogen bonding of two discrete charged clusters, $[Cu_2(CO_2)_3(H_2O)_2]^+$ and $[Cu(CO_2)_3]^-$. Here, hydrogen bonding occurs between water molecules and monodentate carboxylate functionalities from the CPB linker (center-to-center oxygen distance in the range of 2.563−2.740 Å; Figure 4A). It is noted that DEF ligands are present in both the discrete cluster and infinite rod SBUs. Although the infinite rod and discrete cluster SBUs have similar chemical formulas, their geometries are distinctly different. Accordingly, a 3D framework with the new **hhp** topology results from the linking of infinite rods with trigonal-prismatic (discrete Cu_3 clusters) and hexagonal (CPB linker) SBUs (Figure 4B,C). This is the first framework with a topology derived from a combination of discrete and rod-shaped SBUs in one structure (SI, section S4).

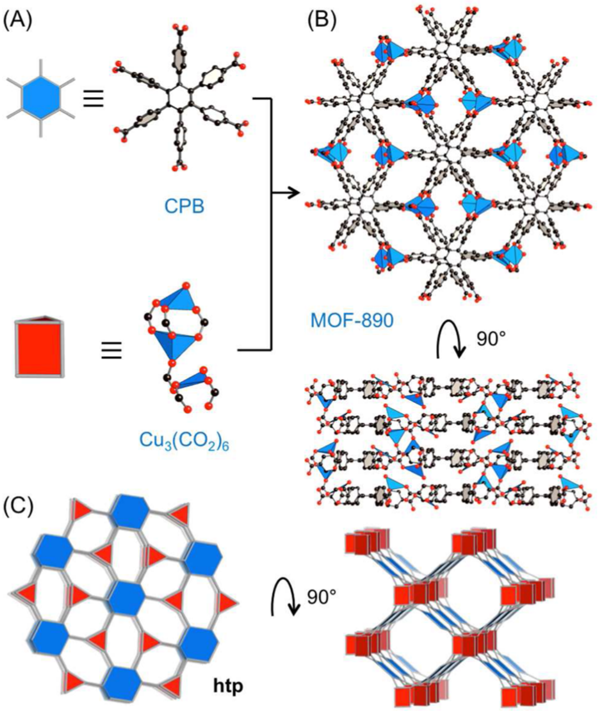

Figure 3. Crystal structure of MOF-890. (A) Linking of hexagonal CPB and trigonal-prismatic $Cu_3(CO_2)_6$ SBUs resulting in (B) MOF-890. (C) Structure of MOF-890 adopting the **htp** topology. This is the first framework with a topology composed of both hexagonal and trigonal-prismatic SBUs. Color code: Cu, blue polyhedra; C, black, O, red. All H atoms are omitted for clarity.

2. Structural Robustness and Permanent Porosity. The successful synthesis of highly crystalline and phase-pure MOF-888, MOF-889, MOF-890, and MOF-891 was confirmed by PXRD analysis of the as-synthesized materials in comparison with the simulated pattern generated from the single-crystal structures (SI, section S5, Figures S9−S12). The as-synthesized MOFs were subsequently washed with DMF to remove any unreacted species and then exchanged with either DCM (for MOF-888 and -889) or MeOH (for MOF-890 and -891). In order to yield guest-free materials, occluded solvent molecules were removed under reduced pressure at room temperature, followed by heating at 80 °C for 6 h, at 120 °C for 6 h, and finally at 180 °C for 24 h. Structural maintenance after activation was proven by PXRD analysis, in which the peak positions of the activated samples were coincident to both the as-synthesized and simulated patterns (SI, Figures S9−S12).

The thermal robustness of MOF-888−MOF-891 was demonstrated by performing TGA (SI, section S6). For activated MOF-888 and -889, the TGA curves under airflow exhibited no appreciable weight loss up to 350 and 400 °C, thus highlighting the high thermal stability of these materials (SI, Figures S13 and S14). In the TGA curves for MOF-890 and -891, a weight loss of 3.06 and 4.52% was observed from room

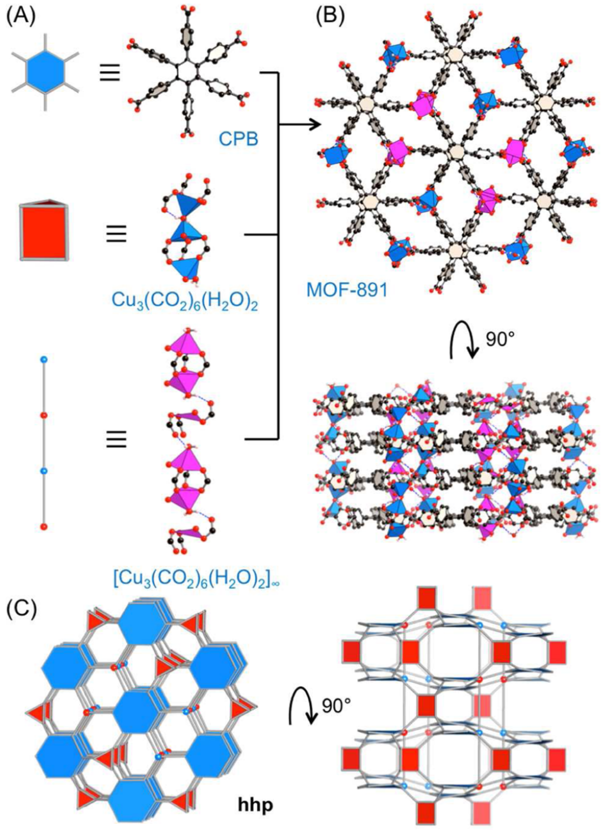

Figure 4. Crystal structure of MOF-891. (A) Linking of hexagonal CPB, trigonal-prismatic $Cu_3(CO_2)_6(H_2O)_2$, and infinite $[Cu_3(CO_2)_6(H_2O)_2]_\infty$ (red and blue binodal rods) SBUs resulting in (B) MOF-891. (C) Structure of MOF-891 adopting the **hhp** topology. This is the first framework with a topology derived from a combination of discrete and rod-shaped SBUs in one structure. Color code: Cu, blue polyhedra; C, black, O, red. All H atoms, except for those participating in hydrogen bonding, are omitted for clarity.

temperature to 100 °C, corresponding to exchanged solvent MeOH molecules in the channels, with framework decomposition occurring at 300 °C (SI, Figures S15 and S16). Finally, analysis of the weight percent of residual metal oxide for MOF-888 (13.5%), MOF-889 (8.99%), MOF-890 (22.5%), and MOF-891 (23.8%) was found to be consistent with the calculated value derived from EA (16.5, 8.45, 22.2, and 22.8%, respectively).

The permanent porosity of all members of this series was evaluated by measuring N_2 adsorption isotherms at 77 K using activated materials. The resulting N_2 isotherms exhibited typical type I behavior, indicative of microporosity (SI, Figure S17). From these isotherms, the BET/Langmuir surface areas for MOF-888, MOF-889, MOF-890, and MOF-891 were estimated to be 40/70, 140/160, 300/340, and 200/240 $m^2\ g^{-1}$, respectively. These measurements are in line with the theoretical accessible surface areas calculated for MOF-888, MOF-889, MOF-890, and MOF-891 (60, 125, 450, and 290 $m^2\ g^{-1}$, respectively).

3. Gas Adsorption Properties. *Thermodynamic Uptake Capacity.* Single-component gas adsorption isotherms (CO_2, N_2, and CH_4) were measured at 273, 283, and 298 K for all members of this series (SI, Figures S18−S29). As shown in Table 2, MOF-890 and MOF-891 display the highest CO_2 capacities (58 $cm^3\ g^{-1}$) at 800 Torr and 298 K. This is in contrast to the N_2 and CH_4 uptake capacities observed for MOF-890 (6.0 and 24 $cm^3\ g^{-1}$, respectively) and MOF-891 (6.4 and 30 $cm^3\ g^{-1}$, respectively) at the same temperature and pressure, which demonstrates the potential of these MOFs for CO_2 storage and separation (Figure 5 and SI, section S7).

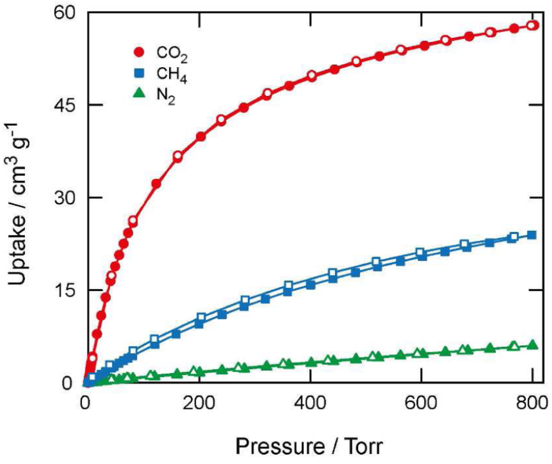

Figure 5. CO_2 (blue), CH_4 (red), and N_2 (green) isotherms for MOF-890 at 298 K. Filled and open symbols represent adsorption and desorption branches, respectively. The connecting curves are guides for the eye.

MOF-889 also displayed relatively moderate uptake capacities for CO_2 and CH_4 (55 and 26 $cm^3\ g^{-1}$, respectively) in comparison with a low N_2 capacity (5.3 $cm^3\ g^{-1}$) at 800 Torr and 298 K (Table 2 and SI, section S7). Furthermore, for MOF-888, MOF-889, MOF-890, and MOF-891, the initial uptake in the low-pressure region of the CO_2 isotherms at 298 K is much steeper than those observed for N_2 or CH_4. This is indicative of the MOF frameworks' higher affinity to CO_2 (Figure 5 and SI, section S7).

Coverage-Dependent Isosteric Heat of Adsorption and Gas Selectivity. Motivated by these observations, we sought to

Table 2. Surface Area, Thermodynamic CO_2 Uptake Capacity, and CO_2/N_2 and CO_2/CH_4 Selectivities for MOF-888, -889, -890, and -891

MOF	A_{BET} ($m^2\ g^{-1}$)[a]	CO_2 uptake ($cm^3\ g^{-1}$)[b]	N_2 uptake ($cm^3\ g^{-1}$)[b]	CH_4 uptake ($cm^3\ g^{-1}$)[b]	isosteric heat of CO_2 adsorption (kJ mol^{-1})[c]	CO_2/N_2 selectivity[d]	CO_2/CH_4 selectivity[d]
MOF-888	38	24	1.8	12	34	57	6.8
MOF-889	144	55	5.3	26	28	25	3.9
MOF-890	295	58	6.0	24	31	63	9.0
MOF-891	200	58	6.4	30	34	56	7.2

[a] Calculated by the BET method. [b] At 800 Torr and 298 K. [c] Calculated by a virial-type expansion equation at near-zero CO_2 coverage. [d] Calculated from pure-component isotherms by Henry's law.

analyze the applicability of MOF-889, -890, and -891 in the industrially relevant flue and natural gas purification processes.[21] Accordingly, the coverage-dependent isosteric heat of adsorption (Q_{st}) for CO_2, N_2, and CH_4 were calculated by fitting the respective isotherms at 273, 283, and 298 K using a virial-type expansion equation (SI, Figures S30 and S31).[22] As shown in Table 2, all members of this series exhibited relatively high CO_2 adsorption enthalpies at zero coverage (34, 28, 31, and 34 kJ mol^{-1} for MOF-888, -889, -890, and -891, respectively; SI, Figure S30). For perspective, the Q_{st} values calculated for MOF-888, -890, and -891 are greater than other well-known MOFs, such as NOTT-140 and HKUST-1 (hydrate; 25 and 30 kJ mol^{-1}, respectively) but slightly less than those of MIL-53(Al) and Co-MOF-74 (35 and 37 kJ mol^{-1}, respectively).[22] Unsurprisingly, these values were substantially higher than the values calculated for N_2 and CH_4 (SI, Figures S30 and S31). These results led, in turn, to estimation of the CO_2/N_2 and CO_2/CH_4 selectivities using Henry's law (Table 2 and SI, section S7). MOF-890 exhibits the highest selectivity in this series toward CO_2 in binary mixtures containing either N_2 or CH_4 (63 and 9.0 for CO_2/N_2 and CO_2/CH_4, respectively). The other members of this series also demonstrate high selectivities for such binary mixtures, as depicted in Table 2.[23] To prove the validity of these calculations and definitively demonstrate the CO_2 separation properties of these materials, dynamic breakthrough experiments were subsequently performed.[21]

Dynamic Adsorption Capacity via Breakthrough Measurements. Breakthrough measurements were performed on MOF-890 as a representative example (SI, section S8). In a typical experiment, a bed packed with MOF-890 was exposed to binary gas streams containing dry mixtures of CO_2/N_2 (16:84, v/v) or CO_2/CH_4 (20:80, v/v) at room temperature (Figure 6). In both cases, it was clearly observed that only CO_2 was retained in the pores, while either N_2 or CH_4 passed through. From these measurements, the dynamic CO_2 uptake capacities in the CO_2/N_2 and CO_2/CH_4 separation were 31 (6.1) and 25 (4.9) $cm^3\ g^{-1}$ (wt %), respectively (Table 3). In comparison with that of BPL carbon, which is widely used in industry because of its ease of desorption and regeneration, MOF-890 exhibited a longer CO_2 retention time for both measurements (Table 3 and SI, Figures S32−S35), indicating higher CO_2 capacities. To prove the recyclability of MOF-890, breakthrough measurements were performed over three consecutive cycles (SI, Figures S32 and S34). Remarkably, there was no observable loss in the separation performance of MOF-890 in either the CO_2/N_2 or CO_2/CH_4 measurements. Furthermore, it was demonstrated that, by simply flowing pure N_2 or CH_4 gas, respectively, through the MOF-loaded bed, MOF-890 could be fully regenerated.

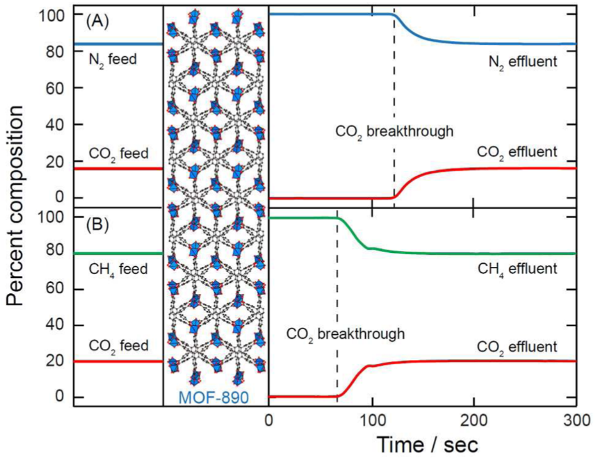

Figure 6. Binary mixture of CO_2/N_2 (A) or CO_2/CH_4 (B) flowed through a fixed bed of MOF-890. The breakthrough time is indicated by the dashed line.

Table 3. Dynamic CO_2 Uptake Capacity for MOF-890

	CO_2/N_2[a]		CO_2/CH_4[b]	
material	uptake capacity ($cm^3\ g^{-1}$)	uptake capacity (wt %)	uptake capacity ($cm^3\ g^{-1}$)	uptake capacity (wt %)
MOF-890	31	6.1	25	4.9
BPL	18	3.5	11	2.1

[a]Composition: 16:84, v/v. [b]Composition: 20:80, v/v.

■ SUMMARY

In this work, we have demonstrated the synthesis and full characterization of a series of MOFs constructed from a novel, highly symmetric hexatopic linker. Interestingly, the underlying topologies of two members of this series, notably MOF-890 with **htp** topology and MOF-891 with **hhp** topology, were found to be new. MOF-888, MOF-889, MOF-890, and MOF-891 were shown to have moderately high CO_2 uptake capacities at 800 Torr and 298 K (55, 58, and 58 $cm^3\ g^{-1}$, respectively) with correspondingly high isosteric heats of CO_2 adsorption at zero coverage (28, 31, and 34 kJ mol^{-1}, respectively). Motivated by these findings, breakthrough measurements were performed on MOF-890, as a representative example, to demonstrate its capability of separating CO_2 from binary gas mixtures containing either N_2 or CH_4. As expected, MOF-890 was an effective adsorbent for such separations (6.1 and 4.9 wt % CO_2 capacity for CO_2/N_2 and CO_2/CH_4 separations, respectively) and was shown to be effective over three consecutive cycles with minimal energy input needed for regeneration (simple N_2 or CH_4 flow).

■ ASSOCIATED CONTENT

Ⓢ Supporting Information

The Supporting Information is available free of charge on the ACS Publications website at DOI: 10.1021/acs.inorgchem.5b01900.

Linker synthesis and characterization, full MOF synthetic details and characterization (including PXRD, TGA curves, and adsorption isotherms), and the experimental conditions for breakthrough measurements (PDF)
Crystallographic data in CIF format (CIF)
Crystallographic data in CIF format (CIF)
Crystallographic data in CIF format (CIF)
Crystallographic data in CIF format (CIF)

■ AUTHOR INFORMATION

Corresponding Authors

*E-mail: kcordova@berkeley.edu.
*E-mail: furukawa@berkeley.edu.

Author Contributions

§P.T.K.N. and H.T.D.N. contributed equally.

Notes

The authors declare no competing financial interest.

■ ACKNOWLEDGMENTS

Prof. O. M. Yaghi is gratefully acknowledged for founding and supporting MANAR. We acknowledge T. T. Ho and A. M. Osborn at MANAR for valuable discussion and assistance on this work. We thank Dr. H. T. C. Ho, Dr. Q. T. Ton, and Prof. H. T. Nguyen at the University of Science (VNU—HCM) for their valuable input. We are indebted to Prof. M. O'Keeffe (Arizona State University) for useful discussion on topological analysis. The work was supported for the synthesis and general adsorption characterization by VNU—HCM (Nos. B2011-50-01TĐ and A2015-50-01-HĐ-KHCN), and the dynamic breakthrough measurement was supported by the United States Office of Naval Research Global: Naval International Cooperative Opportunities in Science and Technology Program (No. N62909-15-1N056). J.K. acknowledges support from the Mid-Career Researcher Program of the National Research Foundation of Korea funded by the Ministry of Science, ICT, and Future Planning (NRF-2014R1A2A1A11054190).

■ REFERENCES

(1) Furukawa, H.; Cordova, K. E.; O'Keeffe, M.; Yaghi, O. M. *Science* **2013**, *341*, 1230444.

(2) (a) Guillerm, V.; Kim, D.; Eubank, J. F.; Luebke, R.; Liu, X.; Adil, K.; Lah, M. S.; Eddaoudi, M. *Chem. Soc. Rev.* **2014**, *43*, 6141−6172. (b) O'Keeffe, M.; Yaghi, O. M. *Chem. Rev.* **2012**, *112*, 675−702. (c) Li, M.; Li, D.; O'Keeffe, M.; Yaghi, O. M. *Chem. Rev.* **2014**, *114*, 1343−1370.

(3) (a) Zhang, Y.-B.; Furukawa, H.; Ko, N.; Nie, W.; Park, H. J.; Okajima; Cordova, K. E.; Deng, H.; Kim, J.; Yaghi, O. M. *J. Am. Chem. Soc.* **2015**, *137*, 2641−2650. (b) Mason, J. A.; McDonald, T. M.; Bae, T.-H.; Bachman, J. E.; Sumida, K.; Dutton, J. J.; Kaye, S. S.; Long, J. R. *J. Am. Chem. Soc.* **2015**, *137*, 4787−4803. (c) Nguyen, N. T. T.; Furukawa, H.; Gándara, F.; Nguyen, H. T.; Cordova, K. E.; Yaghi, O. M. *Angew. Chem., Int. Ed.* **2014**, *53*, 10645−10648.

(4) (a) Mondloch, J. E.; Katz, M. J.; Isley, W. C., III; Ghosh, P.; Liao, P.; Bury, W.; Wagner, G. W.; Hall, M. G.; DeCoste, J. B.; Peterson, G. W.; Snurr, R. Q.; Cramer, C. J.; Hupp, J. T.; Farha, O. K. *Nat. Mater.* **2015**, *14*, 512−516. (b) McGuirk, C. M.; Katz, M. J.; Stern, C. L.; Sarjeant, A. A.; Hupp, J. T.; Farha, O. K.; Mirkin, C. A. *J. Am. Chem. Soc.* **2015**, *137*, 919−925. (c) Choi, K. M.; Na, K.; Somorjai, G. A.; Yaghi, O. M. *J. Am. Chem. Soc.* **2015**, *137*, 7810−7816.

(5) (a) Sun, L.; Hendon, C. H.; Minier, M. A.; Walsh, A.; Dincă, M. *J. Am. Chem. Soc.* **2015**, *137*, 6164−6167. (b) Campbell, M. G.; Sheberla, D.; Liu, S.; Swager, T. M.; Dincă, M. *Angew. Chem., Int. Ed.* **2015**, *54*, 4349−4352.

(6) (a) Ko, N.; Choi, P. G.; Hong, J.; Yeo, M.; Sung, S.; Cordova, K. E.; Park, H. J.; Yang, J. K.; Kim, J. *J. Mater. Chem. A* **2015**, *3*, 2057−2064. (b) Furukawa, H.; Gándara, F.; Zhang, Y.-B.; Jiang, J.; Queen, W. L.; Hudson, M. R.; Yaghi, O. M. *J. Am. Chem. Soc.* **2014**, *136*, 4369−4381.

(7) (a) Zhao, D.; Timmons, D. J.; Yuan, D.; Zhou, H.-C. *Acc. Chem. Res.* **2011**, *44*, 123−133. (b) Lu, W.; Wei, Z.; Gu, Z.-Y.; Liu, T.-F.; Park, J.; Park, J.; Tian, J.; Zhang, M.; Zhang, Q.; Gentle, T., III; Bosch, M.; Zhou, H.-C. *Chem. Soc. Rev.* **2014**, *43*, 5561−5593.

(8) (a) Zou, Y.; Park, M.; Hong, S.; Lah, M. S. *Chem. Commun.* **2008**, 2340−2342. (b) Chen, Z.; Xiang, S.; Liao, T.; Yang, Y.; Chen, Y.-S.; Zhou, Y.; Zhao, D.; Chen, B. *Cryst. Growth Des.* **2010**, *10*, 2775−2779. (c) Zhang, S.-Y.; Zhang, X.; Li, H.; Niu, Z.; Shi, W.; Cheng, P. *Inorg. Chem.* **2015**, *54*, 2310−2314. (d) Duan, X.; Wu, C.; Xiang, S.; Zhou, W.; Yildirim, T.; Cui, Y.; Yang, Y.; Chen, B.; Qian, G. *Inorg. Chem.* **2015**, *54*, 4377−4381. (e) Zhang, H.-M.; Yang, J.; Liu, Y.-Y.; Kang, D.-W.; Ma, J.-F. *CrystEngComm* **2015**, *17*, 3181−3196. (f) He, Y.; Furukawa, H.; Wu, C.; O'Keeffe, M.; Chen, B. *CrystEngComm* **2013**, *15*, 9328−9331.

(9) Chae, H. K.; Eddaoudi, M.; Kim, J.; Hauck, S. I.; Hartwig, J. F.; O'Keeffe, M.; Yaghi, O. M. *J. Am. Chem. Soc.* **2001**, *123*, 11482−11483.

(10) He, Y.; Furukawa, H.; Wu, C.; O'Keeffe, M.; Krishna, R.; Chen, B. *Chem. Commun.* **2013**, *49*, 6773−6775.

(11) Farha, O. K.; Eryazici, I.; Jeong, N. C.; Hauser, B. G.; Wilmer, C. E.; Sarjeant, A. A.; Snurr, R. Q.; Nguyen, S. T.; Yazaydın, A. Ö.; Hupp, J. T. *J. Am. Chem. Soc.* **2012**, *134*, 15016−15021.

(12) (a) Yuan, D.; Zhao, D.; Zhou, H.-C. *Inorg. Chem.* **2011**, *50*, 10528−10531. (b) Yan, Y.; Yang, S.; Blake, A. J.; Lewis, W.; Poirier, E.; Barnett, S. A.; Champness, N. R.; Schröder, M. *Chem. Commun.* **2011**, *47*, 9995−9997. (c) Farha, O. K.; Özgür Yazaydın, A.; Eryazici, I.; Malliakas, C. D.; Hauser, B. G.; Kanatzidis, M. G.; Nguyen, S. T.; Snurr, R. Q.; Hupp, J. T. *Nat. Chem.* **2010**, *2*, 944−948. (d) Peng, Y.; Srinivas, G.; Wilmer, C. E.; Eryazici, I.; Snurr, R. Q.; Hupp, J. T.; Yildirim, T.; Farha, O. K. *Chem. Commun.* **2013**, *49*, 2992−2994.

(13) (a) Jia, J.; Sun, F.; Fang, Q.; Liang, X.; Cai, K.; Bian, Z.; Zhao, H.; Gao, L.; Zhu, G. *Chem. Commun.* **2011**, *47*, 9167−9169. (b) Jia, J.; Wang, L.; Sun, F.; Jing, X.; Bian, Z.; Gao, L.; Krishna, R.; Zhu, G. *Chem. - Eur. J.* **2014**, *20*, 9073−9080. (c) Jia, J.; Sun, F.; Ma, H.; Wang, L.; Cai, K.; Bian, Z.; Gao, L.; Zhu, G. *J. Mater. Chem. A* **2013**, *1*, 10112−10115.

(14) Yuan, D.; Zhao, D.; Sun, D.; Zhou, H.-C. *Angew. Chem., Int. Ed.* **2010**, *49*, 5357−5361.

(15) (a) Tan, C.; Yang, S.; Champness, N. R.; Lin, X.; Blake, A. J.; Lewis, W.; Schröder, M. *Chem. Commun.* **2011**, *47*, 4487−4489. (b) Johnson, J. A.; Lin, Q.; Wu, L.-C.; Obaidi, N.; Olson, Z. L.; Reeson, T. C.; Chen, Y.-S.; Zhang, J. *Chem. Commun.* **2013**, *49*, 2828−2830. (c) Shustova, N. B.; Cozzolino, A. F.; Dincă, M. *J. Am. Chem. Soc.* **2012**, *134*, 19596−19599. (d) Pang, J.; Jiang, F.; Wu, M.; Liu, C.; Su, K.; Lu, W.; Yuan, D.; Hong, M. *Nat. Commun.* **2015**, *6*, 7575. (e) Lu, W.; Yuan, D.; Makal, T. A.; Li, J.-R.; Zhou, H.-C. *Angew. Chem., Int. Ed.* **2012**, *51*, 1580−1584.

(16) (a) He, H.; Sun, F.; Jia, J.; Bian, Z.; Zhao, N.; Qiu, X.; Gao, L.; Zhu, G. *Cryst. Growth Des.* **2014**, *14*, 4258−4261. (b) Eubank, J. F.; Mouttaki, H.; Cairns, A. J.; Belmabkhout, Y.; Wojtas, L.; Luebke, R.; Alkordi, M.; Eddaoudi, M. *J. Am. Chem. Soc.* **2011**, *133*, 14204−14207.

(17) (a) Mio, M. J.; Kopel, L. C.; Braun, J. B.; Gadzikwa, T. L.; Hull, K. L.; Brisbois, R. G.; Markworth, C. J.; Grieco, P. A. *Org. Lett.* **2002**, *4*, 3199−3202. (b) Kobayashi, K.; Shirasaka, T.; Horn, E.; Furukawa, N. *Tetrahedron Lett.* **2000**, *41*, 89−93. (c) Kotha, S.; Brahmachary, E.; Lahiri, K. *Eur. J. Org. Chem.* **2005**, *22*, 4741−4767. (d) Ito, S.; Wehmeier, M.; Brand, J. D.; Kübel, C.; Epsch, R.; Rabe, J. P.; Müllen, K. *Chem. - Eur. J.* **2000**, *6*, 4327−4342.

(18) Brese, N. E.; O'Keeffe, M. *Acta Crystallogr., Sect. B: Struct. Sci.* **1991**, *47*, 192−197.

(19) Blatov, V. A.; Shevchenko, A. P.; Proserpio, D. M. *Cryst. Growth Des.* **2014**, *14*, 3576−3586.

(20) (a) James, M.; Attfield, J. P.; Rodriguez-Carvajal, J. *Chem. Mater.* **1995**, *7*, 1448−1452. (b) Kim, S.-J.; Demazeau, G.; Alonso, J. A.; Choy, J.-H. *J. Mater. Chem.* **2001**, *11*, 487−492. (c) Kogut, E.; Wiencko, H. L.; Zhang, L.; Cordeau, D. E.; Warren, T. H. *J. Am. Chem. Soc.* **2005**, *127*, 11248−11249. (d) Xiao, Z.; Patrick, B. O.; Dolphin, D. *Inorg. Chem.* **2003**, *42*, 8125−8127.

(21) (a) Kizzie, A. C.; Wong-Foy, A. G.; Matzger, A. J. *Langmuir* **2011**, *27*, 6368−6373. (b) Krishna, R.; Long, J. R. *J. Phys. Chem. C* **2011**, *115*, 12941−12950. (c) Remy, T.; Peter, S. A.; Van der Perre, S.; Valvekens, P.; De Vos, D. E.; Baron, G. V.; Denayer, J. F. M. *J. Phys. Chem. C* **2013**, *117*, 9301−9310. (d) Nugent, P.; Belmabkhout, Y.; Burd, S. D.; Cairns, A. J.; Luebke, R.; Forrest, K.; Pham, T.; Ma, S.; Space, B.; Wojtas, L.; Eddaoudi, M.; Zaworotko, M. J. *Nature* **2013**, *495*, 80−84.

(22) (a) Sumida, K.; Rogow, D. L.; Mason, J. A.; McDonald, T. M.; Bloch, E. D.; Herm, Z. R.; Bae, T.-H.; Long, J. R. *Chem. Rev.* **2012**, *112*, 724−781. (b) Furukawa, H.; Miller, M. A.; Yaghi, O. M. *J. Mater. Chem.* **2007**, *17*, 3197−3204.

(23) As stated, the CO_2/N_2 and CO_2/CH_4 selectivities are calculated using Henry's constant (initial slope at zero coverage). Thus, the selectivity is dependent on the low-pressure gas uptake as opposed to the uptake at 800 Torr. Considering that the CO_2 uptake in MOF-890

at ~55 Torr (20 cm^3 g^{-1}) is almost twice as high as that observed for MOF-889 at the same pressure, it is reasonable for MOF-890 to exhibit greater CO_2/N_2 and CO_2/CH_4 selectivities than MOF-889.